Noncatalytic Gas-Solid Reactions in a Vertical Pneumatic Transport Reactor

A heterogeneous model is developed to account for noncatalytic gas-solid reactions in a vertical pneumatic transport reactor. The model takes into consideration both the positive and negative variations of the solid porosity and the variation of the gas diffusivity with the reaction. The method of lines utilizing the second order centered finite difference scheme for the spatial discretization is employed to obtain the model solution.

Experiments utilizing a vertical pneumatic transport reactor of a laboratory scale are performed to study the reaction between limestone and sulfur dioxide generated from coal combustion. The reactor is of 16.2 cm ID and 610 cm in length. The experimental data for sulfur retention are reported for various superficial gas velocities and calcium-sulfur molar ratios. Verification of the model with experimental data is conducted. The agreement between the model prediction and experimental data is satisfactory.

LIANG-SHIH FAN
and SUNIL SATIJA
Department of Chemical Engineering
The Ohio State University
Columbus, OH 43210

B. C. KIM and H. NACK
Battelle's Columbus Laboratories
Columbus, OH 43210

SCOPE

The vertical pneumatic transport reactor has been widely utilized for catalytic fluid reactions and noncatalytic fluid-solid reactions. Reported modeling efforts on the reactant conversion in the reactor have been mainly concerned with the catalytic fluid reactions. Little modeling effort, however, has been placed on the noncatalytic fluid-solid reactions in the reactor. Furthermore, little experimental information is available on the reactor performance for either catalytic fluid reactions or noncatalytic fluid-solid reactions in the literature.

In this paper, a heterogeneous model for a noncatalytic gas-solid reaction in the vertical pneumatic transport reactor is developed. The model takes into account the empirical correlations for the hydrodynamic properties, gas-film diffusion around the solid particle and variation of the gas diffusivity in the particle during the reaction. The effects of various operating parameters of the reactor on the reactant conversion are analyzed. Experiments utilizing a vertical pneumatic transport reactor are also carried out to study the noncatalytic gas-solid reaction. The reaction selected for the study is the sulfation reaction between limestone and sulfur dioxide which is generated from coal combustion. Model verification with the experimental data is conducted.

CONCLUSIONS AND SIGNIFICANCE

A heterogeneous model for a noncatalytic gas-solid reaction in the vertical pneumatic transport reactor is developed. Numerical simulation is made of the effects of various operating parameters on the conversion of the gas and solid reactants. The results indicate that the gas reactant conversion increases with the increase of the solid flow rate, the decrease of the gas superficial velocity, and the increase of the reaction rate constant. Increasing the particle diameter would either increase or decrease the gas reactant conversion, depending on the rate of diffusion in the particle.

Experiments are conducted using a 16.2 cm ID and 610 cm in length vertical pneumatic transport reactor in which limestone is reacted with SO_2 generated from coal combustion. The sulfur retention of limestone particle is found to increase with the decrease of the gas superficial velocity and the increase of calcium/sulfur molar ratios. Model verification is conducted with the experimental data obtained in this study.

INTRODUCTION

The vertical pneumatic transport reactor, known as the riser, has been widely utilized for catalytic fluid reactions such as cracking of gas oil and residue to gasoline (Stemerding, 1962; Bryson et al., 1972). It has also been utilized for noncatalytic fluid-solid reactions such as gasification and combustion of coal and biomass (Nack et al., 1977) and the calcination of aluminum hydroxide (Reh, 1972).

There are several models available to account for the reactant conversion in the vertical pneumatic transport reactor for catalytic reactions (Pratt, 1974; Paraskos et al., 1976; Varghese and Verma, 1979; Fan, 1980, 1981; Fan and Hwang, 1981). Basically, they can be classified into two types: the homogeneous model and the heterogeneous model. The homogeneous model (Paraskos et al., 1976; Fan, 1980, 1981) is used when the Thiele modulus, defined as $(d_p/2)(k_v/D_{eA})^{1/2}$, is less than 1.0, while the heterogeneous model (Pratt, 1974; Varghese and Verma, 1979; Fan and Hwang, 1981) is used when the Thiele modulus is greater than 1.0. The models of Fan (1980, 1981) and Fan and Hwang (1981) incorporate the true hydrodynamic properties which are obtained empirically, including the linear velocity of the gas and solid particle, slip velocity, and void fraction. Other models (Pratt, 1974; Paraskos et al., 1976; Varghese and Verma, 1979), however, impose simplified

Correspondence concerning this paper should be addressed to Liang-Shih Fan.

assumptions on the hydrodynamic properties; for example, the slip velocity is equal to zero or is equal to the particle terminal velocity. In contrast to the efforts on modeling catalytic reactions in the vertical pneumatic transport reactor, little has been done on modeling the noncatalytic reactions in the reactor. Recently, Hartke et al., (1981) performed experiments on the thermal decomposition of $NaHCO_3$ in a laboratory-scale circulating fluidized bed reactor. The results for the rate constants obtained were compared with those obtained in a rotary kiln, a conventional fluidized bed and a pneumatic transport reactor. High decomposition rates were found in the circulating fluidized bed reactor and in the pneumatic transport reactor. A simple, modified shrinking core model was formulated to account for the rate-determining step of $NaHCO_3$ decomposition.

In this paper, a heterogeneous model for a noncatalytic gas-solid reaction in the vertical pneumatic transport reactor is developed. The model takes into account the empirical correlations for the hydrodynamic properties and gas-film diffusion around the solid particle. Both the positive and the negative variations of the solid porosity and the variation of the gas diffusivity with the reaction are considered in the model. The effect of various operating parameters including the superficial gas velocity, length of the reactor, reaction rate constant, particle size, and effective diffusivity on the reactant conversion are analyzed. Experiments utilizing a vertical pneumatic transport reactor are also carried out to study the noncatalytic gas-solid reaction. The reaction selected for the study is the sulfation reaction between limestone and sulfur dioxide which is generated from coal combustion. Model verification with the experimental data is conducted.

THE MODEL

Consider a gas-solid reaction of the following form:

$$\underset{\text{(gas reactant)}}{aA} + \underset{\text{(solid reactant)}}{S_s} \rightarrow \underset{\text{(gas products)}}{\sum_i b_i B_i} + \underset{\text{(solid products)}}{\sum_j C_j S_j}$$

The reaction takes place in an isothermal vertical pneumatic transport reactor. Assume that the entrance effect can be neglected, the gas and solid flows follow the plug flow pattern, and the solid particles are spherical and uniform in size (Fan, 1981). A material balance of the gas reactant in the gas phase give rise to

$$U_g \epsilon_b \frac{dC_1}{dz} + \frac{3(1-\epsilon_b)k_d}{r_0}(C_1 - C_{2|r=r_0}) = 0 \tag{1}$$

where ϵ_b is the void fraction in the bed. The boundary condition for Eq. 1 is

$$z = 0;\ C_1 = C_0 \tag{2}$$

A material balance of the gas reactant and the solid reactant in the solid phase yields, respectively:

$$U_p \frac{\partial(C_2\epsilon)}{\partial z} = \frac{1}{r^2}\frac{\partial}{\partial r}(D_{eA} r^2 \frac{\partial C_2}{\partial r}) - a\tilde{\gamma}_s \tag{3}$$

$$U_p \frac{\partial C_s}{\partial z} = -\tilde{\gamma}_s \tag{4}$$

The boundary conditions for Eqns. 3 and 4 are:

$$\begin{aligned} z = 0;\ C_2 &= 0 \\ C_s &= C_{s0} \end{aligned} \tag{5}$$

$$r = 0;\ \frac{\partial C_2}{\partial r} = 0 \tag{6}$$

$$r = r_0;\ D_{eA}\frac{\partial C_2}{\partial r} = k_d(C_1 - C_2) \tag{7}$$

ϵ in Eq. 3 is the void fraction of the particle. It is assumed that over a given range of the solid conversion, relationship between ϵ and the solid concentration can be approximated by (Wen, 1968; Fan et al., 1977):

$$\epsilon = \epsilon_0 + \gamma\left(1 - \frac{C_s}{C_{s0}}\right) \tag{8}$$

where ϵ_0 is the void fraction of the particle at the initial condition. γ is the parameter for void fraction variation, which is a positive or negative constant. Positive constant for γ accounts for the increase of the void fraction during the reaction. Examples of the reactions with γ as a positive value are ore roasting, coal gasification and combustion, coal desulfurization, calcination, catalyst deactivation, propellent combustion, coal liquefaction, and sodium thiosulfate manufacture. Negative constant for γ accounts for the decrease of the void fraction during the reaction. Examples of the reactions with γ as a negative value are sulfation of limestone, and oxidation, halogenation and sulfidation of metal or alloy.

Effective diffusivity D_{eA} in Eq. 3 accounts for the overall rate of gas diffusion in the porous particle of solid reactant. It is a complex entity constantly changing with variations in the characteristics of the pore network such as pore shape, pore size, and pore size distribution, and with variations in the physical conditions such as temperature and pressure. For gaseous diffusion in porous particle, experimental studies have revealed that the ratio of effective diffusivity to ordinary diffusivity, is changed proportional to $\epsilon^{1.3}$ when bulk diffusion is predominate (Currie, 1960) and proportional to $\epsilon^{2\sim3}$ when Knudsen diffusion is predominant (Weisz and Schwartz, 1962). Furthermore, the micropore model (Wakao and Smith, 1962) asserts that the effective diffusivity is proportional to ϵ^2 if the existence of micropores prevails in the system. For the diffusion of sulfur dioxide in calcium oxide particle, a simple relation was used by Hartman and Coughlin (1976) and Fan et al. (1981), which has the form

$$D_{eA} = D_m \epsilon \tag{9}$$

where D_m is the molecular diffusivity divided by the tortuosity. D_{eA} can be related to D_{eA0} by

$$D_{eA} = D_{eA0}\frac{\epsilon}{\epsilon_0} \tag{10}$$

Equation 10 is used in this study to account for the diffusivity variation with the void fraction in the particle.

$\tilde{\gamma}_s$ is the rate of the solid reactant consumption and can be expressed by

$$\tilde{\gamma}_s = k_v C_2^n C_s^m \tag{11}$$

where k_v is the volumetric rate constant.

The conversion for the solid reactant is defined as

$$X_s = 1 - \frac{\int_v C_s dv}{\int_v C_{s0} dv} \tag{12}$$

The gas reactant conversion in the reactor outlet can be evaluated by

$$X = 1 - \frac{U_g \epsilon_b C_1 + U_p(1-\epsilon_b)\overline{C}_2}{U_{gs} C_0} \tag{13}$$

where $\overline{C}_2$ is the average gas reactant concentration in the solid particles which can be expressed by

$$\overline{C}_2 = \frac{3}{r_0^3}\int_0^{r_0} \epsilon C_2 r^2 dr \tag{14}$$

In dimensionless forms, Eqns. 1 through 7 respectively become:

$$\frac{df_1}{dy} + F(f_1 - f_{2|x=1}) = 0 \tag{15}$$

$$y = 0;\ f_1 = 1 \tag{16}$$

$$A\frac{\partial(\epsilon f_2)}{\partial y} = \frac{1}{x^2}\frac{\partial}{\partial x}\left(D_A x^2 \frac{\partial f_2}{\partial x}\right) - \phi_v^2 f_2^n g_1^m \tag{17}$$

$$\frac{\partial g_1}{\partial y} = -G f_2^n g_1^m \tag{18}$$

$$y = 0; \begin{matrix} f_2 = 0 \\ g_1 = 1 \end{matrix} \tag{19}$$

$$x = 0; \frac{\partial f_2}{\partial x} = 0 \tag{20}$$

$$x = 1; D_A \frac{\partial f_2}{\partial x} = N_{Sha}(f_1 - f_2) \tag{21}$$

where

$$A = \frac{r_0^2 U_p}{L D_{eA0}}, \; f_2 = \frac{C_2}{C_0}, \; \phi_v = r_0 \sqrt{\frac{a k_v C_{s0}^m C_0^{n-1}}{D_{eA0}}}$$

$$x = \frac{r}{r_0}, \; F = \frac{3(1-\epsilon_b) k_d L}{U_g \epsilon_b r_0}$$

$$y = \frac{z}{L}, \; f_1 = \frac{C_1}{C_0}, \; g_1 = \frac{C_s}{C_{s0}}, \; G = \frac{k_v C_0^n L C_{s0}^{m-1}}{U_p}$$

$$D_A = \frac{D_{eA}}{D_{eA0}}, \; N_{Sha} = \frac{r_0 k_d}{D_{eA0}}$$

The dimensionless form of Eq. 12 is:

$$X_s = 1 - 3 \int_0^1 g_1 x^2 dx \tag{22}$$

EVALUATION OF HYDRODYNAMIC AND MASS TRANSFER PROPERTIES FOR THE MODEL

The hydrodynamic properties for the pneumatic transport reactor can be obtained from the mass balance or empirical correlations available in literature as:

The mass balance for the solid particle in the reactor yields

$$\epsilon_b = 1 - \frac{4 W_s}{\rho_p \pi D^2 U_p} \tag{23}$$

The linear particle velocity is obtained by (Yang 1977, 1978):

$$U_p = U_g - U_t \sqrt{\left(1 + \frac{f_p U_p^2}{2 g_c D}\right)} \epsilon_b^{4.7} \tag{24}$$

The solid friction factor, f_p, can be obtained by the following empirical correlation equations (Yang, 1978)

$$f_p = 0.0126 \frac{1-\epsilon_b}{\epsilon_b^3} \left[(1-\epsilon_b)\frac{(Re)_t}{(Re)_p}\right]^{-0.979}, \quad \text{for } U_g/U_t > 1.5 \tag{25}$$

$$f_p = 0.041 \frac{1-\epsilon_b}{\epsilon_b^3} \left[(1-\epsilon_b)\frac{(Re)_t}{(Re)_p}\right]^{-1.021}, \quad \text{for } U_g/U_t < 1.5 \tag{26}$$

U_t, the terminal velocity for the solid particle, can be evaluated by (Yang, 1973)

$$U_t = \frac{0.153\, d_p^{1.14} g^{0.71} (\rho_p - \rho_g)^{0.71}}{\mu^{0.43} \rho_g^{0.29}}, \text{ for } 2.0 < (Re)_p < 1{,}000 \tag{27}$$

and

$$U_t = \frac{d_p^2 (\rho_p - \rho_g) g}{18 \mu}, \quad \text{for } (Re)_p \le 0.1 \tag{28}$$

where

$$(Re)_p = \frac{d_p (U_g - U_p) \rho_g}{\mu} \tag{29}$$

Equations 23 through 26 are solved simultaneously to obtain the hydrodynamic properties including ϵ_b, f_p and U_p. The values of ϵ_b and U_p are required for the model equations.

The gas film mass transfer coefficient, k_d, for the suspended solid particles can be obtained by the following empirical correlation equation (Satterfield, 1969):

$$\frac{k_d d_p}{D_M} = 2.0 + 0.63 (Sc)^{1/3} (Re)_p^{1/2} \tag{30}$$

where

$$Sc = \frac{\mu}{\rho_g D_M}$$

METHOD OF SOLUTION

Method

The numerical solution of nonlinear partial differential equations is often highly complicated and frequently unstable. However, this difficulty has been eased by the recent development of a useful and reliable software interface which can eliminate much of the expensive and time-consuming effort involved in the solution of nonlinear partial differential equations (e.g., Sincovec and Madson, 1975). The software interface, which is basically implemented by the so-called "method of lines" (Vichnevetsky, 1971), can provide centered differencing in the spatial variable for time-dependent nonlinear partial-differential equations. This gives a semidiscrete system of nonlinear ordinary differential equations which may then be solved utilizing the recently developed powerful ordinary differential equation integrators.

The present study employs this software interface for numerical calculations. Gear's (1971) backward differentiation is used as the formula for time integration. The modified Newton's method with internally generated Jacobian matrix is utilized to solve the nonlinear equations. Both of them have been combined with the software interface as the load module.

The relative error bound for the time integration process in the present calculation is set at 10^{-2} for each time step, the integrator adjusts the time step size and/or order of the time integration formula to achieve the specified error level. The number of spatial meshes specified for this study is 40.

Comparison with Analytical Solution

The model equation under a special case, namely $n = 1$, $m = 0$, and $\gamma = 0$ can be solved analytically by Laplace transforms. The analytical solutions for the gas reactant concentration in both the gas phase and the solid phase and the solid concentration can be expressed by (Fan and Hwang, 1981).

$$\frac{C_1}{C_0} = 1 - \frac{\mathcal{D}(\beta_0 - \tanh \beta_0)\{\exp(s_0 y) - 1\}}{s_0 h_0} - \sum_{n=1}^{\infty} \frac{A' \mathcal{D}(\gamma_n - \tan \gamma_n)\{1 - \exp(s_n y)\}}{(\phi^2 + \gamma_n^2) h_n} \tag{31}$$

$$\frac{C_2}{C_0} = \frac{1}{x}\left\{\frac{\sinh(\beta_0 x)\exp(s_0 y)}{G_0} + \sum_{n=1}^{\infty} \frac{\sin(\gamma_n x)\exp(s_n y)}{G_n} + \sum_{n=1}^{\infty} \frac{\sin(\delta_n x)\exp(\tau_n y)}{F_n}\right\}, \quad \text{for } x \neq 0 \tag{32a}$$

and

$$\frac{C_2}{C_0} = \frac{\beta_0}{G_0}\exp(s_0 y) + \sum_{n=1}^{\infty} \frac{\gamma_n}{G_n}\exp(s_n y) + \sum_{n=1}^{\infty} \frac{\delta_n}{F_n}\exp(\tau_n y), \quad \text{for } x = 0 \tag{32b}$$

$$\frac{C_s}{C_{s0}} = -\frac{k_v L}{U_p}\frac{C_0}{C_{s0}}\left[\frac{1}{x}\left\{\frac{\sinh(\beta_0 x)\exp(s_0 y)}{s_0 G_0} + \sum_{n=1}^{\infty} \frac{\sin(\gamma_n x)\exp(s_n y)}{s_n G_n} + \sum_{n=1}^{\infty} \frac{\sin(\delta_n x)\exp(\tau_n y)}{\tau_n F_n}\right\}\right] + 1 + \frac{k_v L}{U_p}\frac{C_0}{C_{s0}}\left[\frac{1}{x}\left\{\frac{\sinh(\beta_0 x)}{s_0 G_0} + \sum_{n=1}^{\infty} \frac{\sin(\gamma_n x)}{s_n G_n} + \sum_{n=1}^{\infty} \frac{\sin(\delta_n x)}{\tau_n F_n}\right\}\right], \quad \text{for } x \neq 0 \tag{33a}$$

and

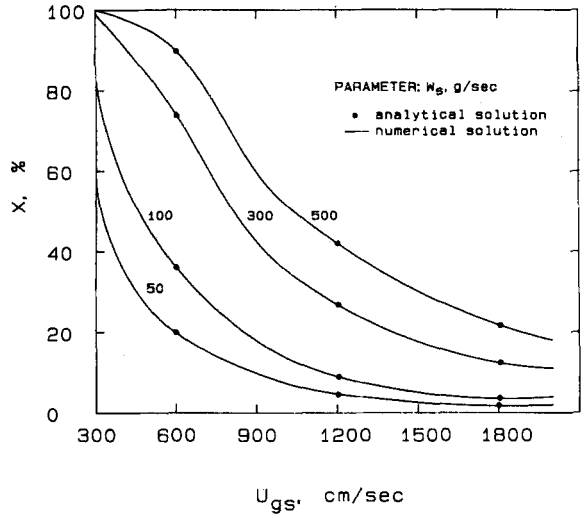

Figure 1. Comparison of the analytical solution and the numerical solution for model.

$$\frac{C_s}{C_{s0}} = -\frac{k_v L}{U_p}\frac{C_0}{C_{s0}}\left[\frac{\beta_0}{G_0 s_0}\exp(s_0 y) + \sum_{n=1}^{\infty}\frac{\gamma_n}{s_n G_n}\exp(s_n y) + \sum_{n=1}^{\infty}\frac{\delta_n}{F_n \tau_n}\exp(\tau_n y)\right] + 1 + \frac{k_v L}{U_p}\frac{C_0}{C_{s0}}\left[\frac{\beta_0}{G_0 s_0} + \sum_{n=1}^{\infty}\frac{\gamma_n}{s_n G_n} + \sum_{n=1}^{\infty}\frac{\delta_n}{F_n \tau_n}\right], \text{ for } x = 0 \quad (33b)$$

where

$$\mathcal{D} = \frac{3(1-\epsilon_b)LD_{eA}}{U_g \epsilon_b r_0^2}, \quad A' = \frac{\epsilon_0 r_0^2 U_p}{LD_{eA}}, \quad E = \frac{1}{N_{Sha}}$$

β_0 is the real root of the following equation:

$$\{E(\beta_0^2 - \phi^2) + A'\mathcal{D}\}\beta_0 = \{A'\mathcal{D} + (E-1)(\beta_0^2 - \phi^2)\}\tanh\beta_0$$

γ_n is the root of the following equation:

$$\tan\gamma_n\{A'\mathcal{D} - (E-1)(\gamma_n^2 + \phi^2)\} = \{A'\mathcal{D} - E(\gamma_n^2 + \phi^2)\}\gamma_n$$

$$s_0 = \frac{(\beta_0^2 - \phi^2)}{A'}, \quad s_n = \frac{-(\phi^2 + \gamma_n^2)}{A'}$$

$$h_0 = (1-E)\tanh\beta_0 + E\beta_0 + (EA' + \mathcal{D}A')/2\beta_0 + \{s_0(1-E) - \mathcal{D}\}A'/(2\beta_0\cosh^2\beta_0)$$

$$h_n = (1-E)\tan\gamma_n + E\gamma_n - (E+\mathcal{D})A'/2\gamma_n + \{(\phi^2 + \gamma_n^2)(1-E) + \mathcal{D}A'\}/(2\gamma_n\cos^2\gamma_n)$$

$$\delta_n = (n - \tfrac{1}{2})\pi$$

$$\tau_n = -(\phi^2 + \delta_n^2)/A'$$

$$G_0 = h_0\cosh\beta_0 + \{s_0[(1-E)\tanh\beta_0 + E\beta_0] + \mathcal{D}(\beta_0 - \tanh\beta_0)\}\begin{pmatrix}A'\\2\beta_0\end{pmatrix}\sinh\beta_0$$

$$G_n = h_n\cos\gamma_n + \{s_n[(1-E)\tan\gamma_n + E\gamma_n] + \mathcal{D}(\gamma_n - \tan\gamma_n)\}\left(\frac{A'}{2\gamma_n}\right)\sin\gamma_n$$

$$F_n = \left\{(1-E) + \frac{(\tau_n E + \mathcal{D})A'}{2}\right\}(-1)^{n+1}$$

As shown in Figure 1, the numerical solutions agree well with the analytical solutions for the special case considered for the model. The values of the parameters used for Figure 1 are given in Table 1.

TABLE 1. NOMINAL VALUES OF THE PARAMETERS EMPLOYED FOR FIGS. 1 AND 3 THROUGH 12

a	= 1 for Figs. 1, 3–12
m	= 0 for Fig. 1 = 1 for Figs. 3–12
n	= 1 for Figs. 1, 3–12
ρ_p	= 2.5 g/cm^3 for Figs. 1, 3–12
ρ_g	= 0.001 g/cm^3 for Figs. 1, 3–12
D	= 7.62 cm for Figs. 1, 3–12
k_v	= 200 s^{-1} for Fig. 1 8000 cm^3/gmol·s for Figs. 5–6, 8, 10–12 500–8,000 cm^3/gmol·s for Figs. 4, 9 500–60,000 cm^3/gmol·s for Figs. 3, 7
D_{eA0}	= 0.1 cm^2/s for Figs. 1, 3, 4, 9–11 0.001–0.1 cm^2/s for Figs. 6, 8, 12 0.0001–0.1 cm^2/s for Fig. 5 0.01 cm^2/s for Fig. 7
W_s	= 50–500 g/s for Figs. 1, 3, 5 300 g/s for Figs. 4, 6, 8, 9, 12 100 and 300 g/s for Fig. 10 50 g/s for Figs. 7, 11
U_{gs}	= 300–2,000 cm/s for Figs. 1, 4 500 cm/s for Figs. 3, 5–12
d_p	= 50 μm for Figs. 1, 3–5, 8, 10–12 20–200 μm for Figs. 6, 7 100 μm for Fig. 9
C_{s0}	= 0.025 gmol/cm^3 for Figs. 1, 3–12
C_0	= 3.25 × 10^{-5} gmol/cm^3 for Figs. 1, 3–12
μ_g	= 1.8 × 10^{-4} g/cm·s for Figs. 1, 3–12
L	= 800 cm for Figs. 1, 3, 4–8, 10–12 2,000 cm for Fig. 9
ϵ_0	= 0.2 for Figs. 1, 3, 4, 8–12 0.6 for Figs. 5, 6, 7
γ	= 0.0 for Fig. 1 0.8 for Figs. 3, 4, 7, 9–11 (−0.8) and 0.8 for Figs. 5, 6 0.0 − 0.8 for Fig. 8 (−0.8) − 0.0 for Fig. 12

EXPERIMENTAL

Experiments are conducted to study the vertical pneumatic transport reactor in which the noncatalytic reaction between limestone and sulfur dioxide is carried out. The schematic diagram of the experimental system is given in Figure 2. The reactor is 16.2 cm ID and 610 cm in length with air as the fluidizing gas. It consists of two sections: dense section and dilute section. Coal and limestones are fed pneumatically into the dense section where combustion of coal takes place. The dense section contains 6 × 12 mesh size heavy particles which serve to retain and distribute coal particles creating adequate mixing for the mass transfer and reaction. Sulfur dioxide is generated during the combustion process, which subsequently reacts with limestone in the reactor. This reaction is required for sulfur emission control.

Heat resulted from the combustion reaction is absorbed by the entrained particles (sand) which are circulated out of the reactor along with the fine particles such as spent limestone and ash. The entrained particles (sand) and parts of spent limestone and ash are then separated from the fine particles and transported to the hot recycle chamber and to the heat exchanger unit for steam generation before circulating back to the reactor. This combustion process is known as "multisolid fluidized bed combustion process," which was originally developed by Battelle Memorial Institute

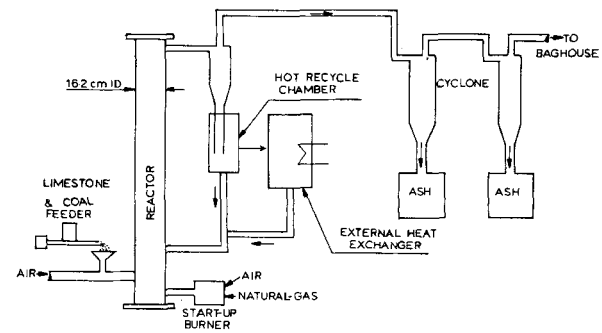

Figure 2. Schematic diagram of the experimental system.

TABLE 2. SPECIFICATION OF MULTISOLID FLUIDIZED-BED COMBUSTION UNIT

Combustor Internal Diameter	: 16.2 cm (6-3/8 in.)
Combustor Height	: 610 cm (20 ft)
Height of Dense Bed (Settled)	: 50.8 cm (20 in.)
Height of Dense Bed (Expanded)	: 101.6 cm (40 in.)
Coal Feed Rate	: 6.3 g/s (50 lb/h)
Sulfur in Coal	: 4%
Sand Circulation Rate	: 63.1 g/s (500 lb/h)
Total Solids Circulation Rate	: 75.8-85.4 g/s (600-690 lb/h)
$CaCO_3$ in Limestone	: 83.6%
Limestone Sorbent Circulation Rate	: 9.47 g/s for Ca/S Molar Ratio = 2 13.89 g/s for Ca/S Molar Ratio = 3 15.78 g/s for Ca/S Molar Ratio = 4 19.73 g/s for Ca/S Molar Ratio = 5
Calcium-Sulfur Molar Ratio	: 2, 3, 4 and 5
Material of Dense Bed	: Iron Ore (Crushed)
Average Bed Temperature	: 868°C
Average Diameter of Limestone Particle	: 16 μm
Residence Time of Limestone Particles in Dense Bed	: ~6 s
Type of Limestone	: Greer Limestone

(Nack et al., 1977). Table 2 details the dimension of the experimental system and the operating conditions considered in the experiment.

RESULTS AND DISCUSSION

The numerical simulation is conducted to account for the general behavior of the noncatalytic gas-solid reactions in the vertical pneumatic transport reactor. Specifically, the general effects of the process variables represented by two major types of noncatalytic gas-solid reactions are considered. These two types of reactions are the solid porosity increasing with the reaction and the solid porosity decreasing with the reaction. The former is characterized by a positive value for γ in the model while the latter is characterized by a negative value for γ in the model. The experimental conditions reported here represent only one type of the noncatalytic gas-solid reaction, namely, the solid porosity decreasing with the reaction. The experiments serve to partially verify the general mathematical model developod in this study.

Numerical Simulation

The results of the numerical simulation based on the model are shown in Figures 3 through 12. The nominal values of the parameters employed in these figures are given in Table 1. Note that the values of ϵ_0 and γ given in Table 1 are applicable only for a limited range of solid conversion considered in this study; extrapolating beyond which would result in values for ϵ which are either negative or over one. Figures 3, 4, and 7 through 11 show the parametric effects of the superficial gas velocity, reaction rate constant, flow rate of the solid particles, length of the reactor, and variation constant of the solid porosity on the reactant conversion for cases involving positive values of γ. The parametric effect of the variation constant of the solid porosity on the reactant conversion for cases involving negative values of γ is described in Figure 12. While the parametric effects of the particle radius and diffusivity of the solid particles on the reactant conversion for cases involving both negative and positive values of γ are described in Figures 5 and 6.

Figure 3 shows the effect of the solid flow rate on the gas conversion as a function of the reaction rate constant. The gas conversion increases with the increase of the flow rate. The effect of the solid flow rate on the gas conversion is more pronounced at the high reaction rate constant. At the reaction rate constant of 8,000 cm^3/gmol-s, the increase in the solid flow rate from 100 to 500 g/s,

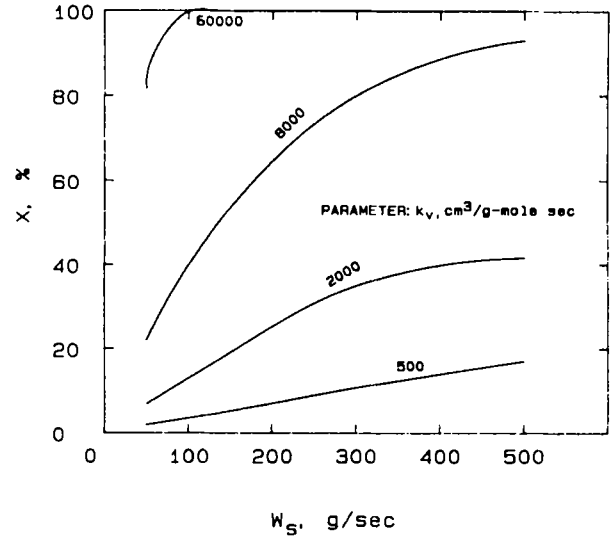

Figure 3. Effect of the solid flow rate on the gas conversion as a function of the reaction rate constant for positive values of γ.

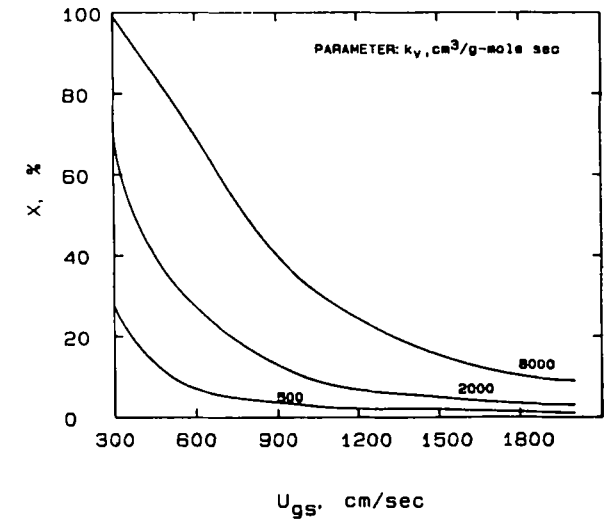

Figure 4. Effect of the superficial gas velocity on the gas conversion as a function of the reaction rate constant for positive values of γ.

gives rise to an increase of the gas conversion from 40 to 93% while at the reaction rate constant of 500 cm^3/gmol-s, the gas conversion increases only from 4 to 17%.

Figure 4 shows the effect of the superficial gas velocity on the gas conversion as a function of three reaction rate constants, i.e., 500, 2,000, 8,000 cm^3/gmol-s. It is seen that the gas conversion decreases with the increase of the gas superficial velocity due to the decrease of the gas residence time in the reactor. It is noted that the increase in the superficial gas velocity from 300 to 900 cm/s reduces the gas conversion from 99 to 40% for the reaction rate constant of 8,000 cm^3/gmol-s.

Figure 5 shows the effect of the initial gas diffusivity in the solid, D_{eA0}, on the gas conversion as a function of the solid flow rate for both positive and negative values of γ. For positive values of γ, it is seen that the gas conversion increases as the solid flow rate increases at a given D_{eA0}. For a given flow rate, the gas conversion increases as D_{eA0} increases to about 0.02 cm^2/s, beyond which, the gas conversion remains practically constant. This signifies that the gas diffusion in the solid is not the rate-determining step in the overall rate of reaction. Note that the Thiele modulus with D_{eA0} of 0.02 cm^2/s is 0.25 indicating that the homogeneous model can be used to account for the reactant conversion in the particle at D_{eA0} beyond 0.02 cm^2/s (Fan et al., 1978). For negative values of

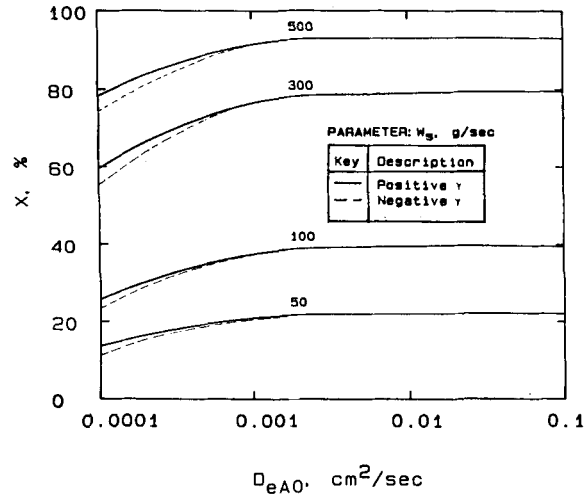

Figure 5. Effect of the initial gas diffusivity in the solid particle on the gas conversion as a function of solid flow rate.

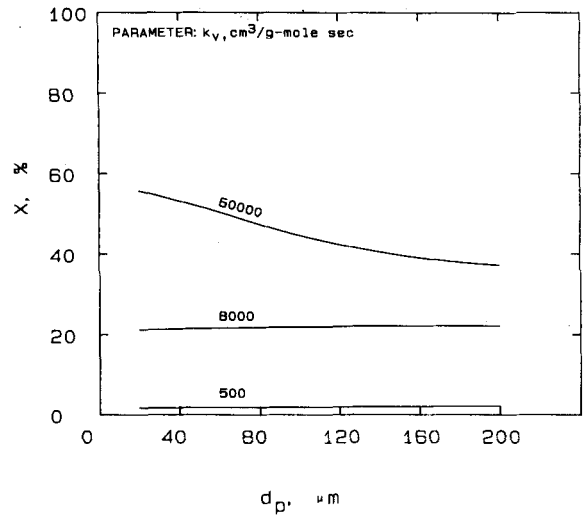

Figure 7. Effect of the particle diameter on the gas conversion as a function of the reaction rate constant for positive values of γ.

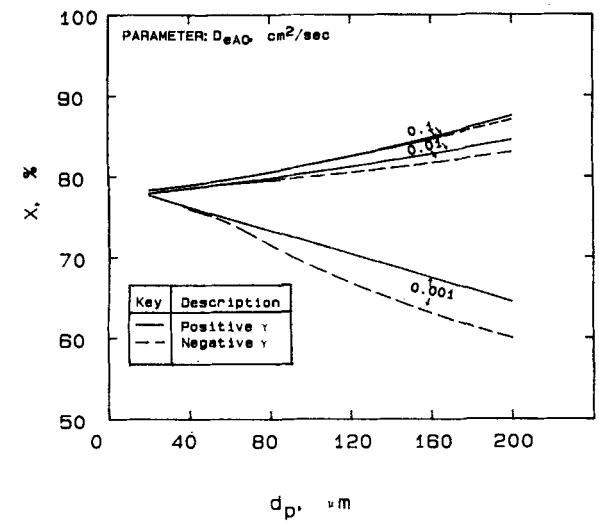

Figure 6. Effect of the particle diameter on the gas conversion as a function of the initial gas diffusivity in the solid particle.

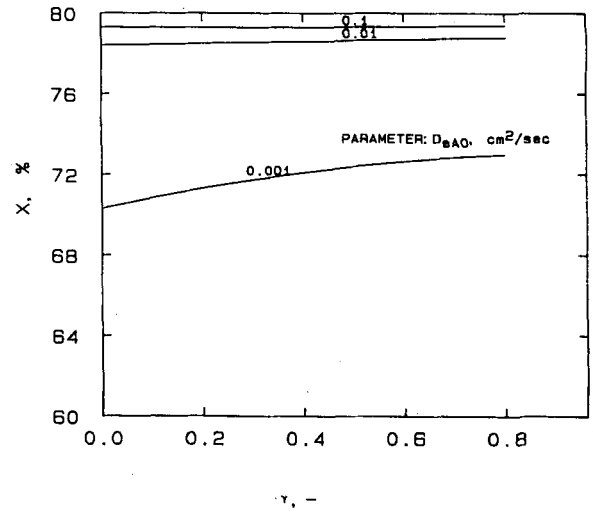

Figure 8. Effect of the positive values of γ on the gas conversion as a function of the initial gas diffusivity in the solid particle.

γ, it is seen that the variation of the gas conversion with D_{eA0} for a given solid flow rate is similar to that for positive values of γ. For D_{eA0} as large as 0.1 cm^2/s, the gas conversion for negative values of γ is identical to that for positive values of γ for a given solid flow rate. However, the differences are observed for the gas conversion between the two cases at D_{eA0} as small as 0.0001.

Figure 6 shows the effect of the particle diameter on the gas conversion as a function of three different values of the initial gas diffusivity in the solid, i.e., 0.001, 0.01 and 0.1 cm^2/s for both positive and negative values of γ. For positive values of γ it is seen that, at D_{eA0} as small as 0.001 cm^2/s, the gas conversion decreases as the particle diameter increases. This is due to the combined effect in that the increase in the particle diameter results in substantial decrease of overall rate of reaction and moderate increase of the hold-up and residence time of the particle. On the other hand, at D_{eA0} as large as 0.1 cm^2/s, the gas conversion increases as the particle diameter increases. This is due to the effect that the increase in the particle diameter results in the essentially unvaried overall rate of reaction and moderate increase of the residence time of the particle. For negative values of γ, the trend of the gas conversion variation with d_p for a given D_{eA0} is similar to that for positive values of γ. No difference of the gas conversion is observed for both negative and positive values of γ at a small d_p.

The effect of the particle diameter on the gas conversion as a function of the reaction rate constant, k_v, is shown in Figure 7. Three values for k_v are considered, i.e., 500, 8,000, and 60,000 cm^3/gmol-s. For the low values of k_v, the overall rate of reaction is predominantly determined by the rate of reaction. Thus, the increase in the particle diameter results in the essentially unvaried overall rate of reaction. However, as described previously, the increase in the particle diameter results in the increase of the residence time and hold-up of the particle in the bed. Thus, it results in a slight increase of the gas conversion as the particle diameter increases for small values of k_v, i.e., 500 and 8,000 cm^3/gmol-s, as shown in Figure 7. For the large values of k_v, the overall rate of reaction is predominantly determined by the rate of diffusion. Thus, the increase in the particle diameter results in the decrease of the overall rate of reaction. This effect combined with the effect of the increase of residence time and holdup of the particle in bed yields the decrease of the gas conversion as the particle diameter increases for a given large value of k_v, i.e., 60,000 cm^3/gmol-s, as shown in Figure 7.

Figure 8 shows the effect of the variation constant of the solid porosity, γ, on the gas conversion as the function of three values of initial gas diffusivity, i.e., 0.001, 0.01, and 0.1 cm^2/s. It can be seen that for D_{eA0} as small as 0.001 cm^2/s, the increase in γ substantially increases the gas conversion. This is because the overall rate of reaction is predominantly determined by the rate of diffusion. The increase in γ increases the rate of diffusion. For D_{eA0}

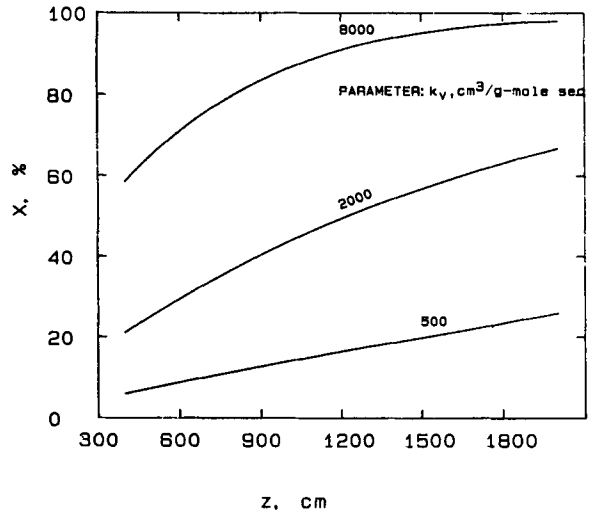

Figure 9. Axial gas conversion profiles as a function of the reaction rate constant for positive values of γ.

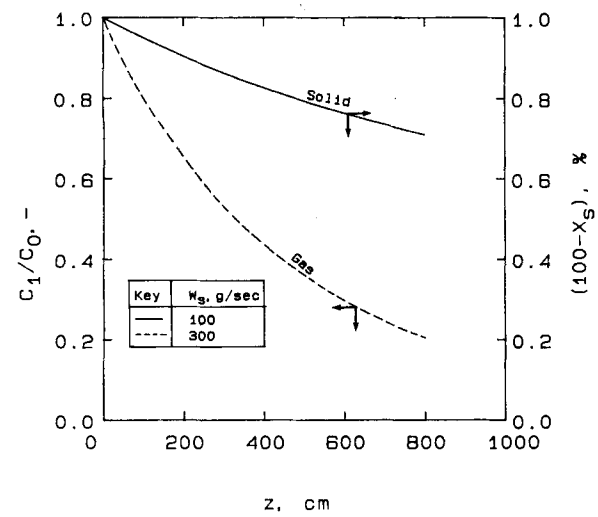

Figure 10. Axial gas and solid reactant concentration profile in the reactor for positive values of γ.

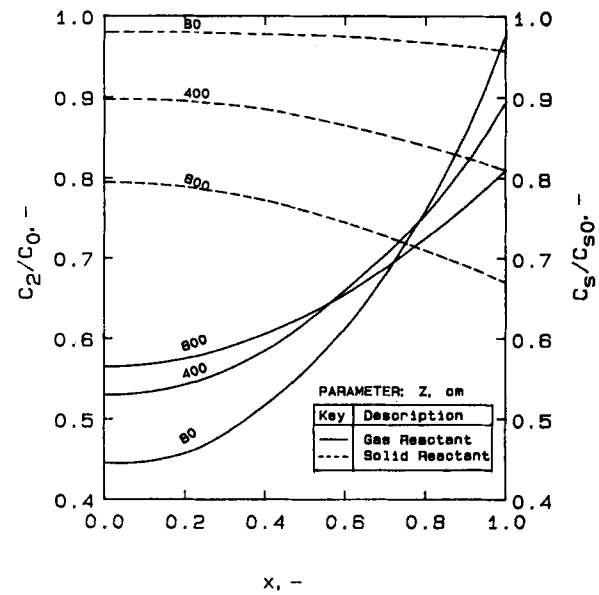

Figure 11. Concentration profile of the gas and the solid reactant in the particle at various locations in the reactor for positive values of γ.

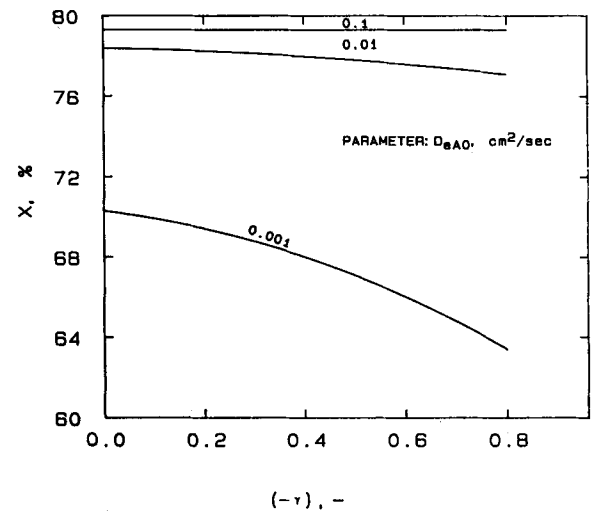

Figure 12. Effect of the negative values of γ on the gas conversion as a function of the initial gas diffusivity in the solid particle.

as large as 0.1 cm^2/s, however, the increase in γ has negligible effect on the gas conversion. This is due to the fact that the overall rate of reaction is predominantly determined by the rate of reaction.

The axial profiles of the gas conversion as a function of three reaction rate constants, i.e., 500, 2,000, and 8,000 cm^3/gmol·s are shown in Figure 9. As expected, at a given location of the reactor, the increase in the reaction rate constant increases the gas conversion. The axial variation of the gas conversion with the distance decreases with the increase of the distance, and this variation is particularly profound for the reaction rate constant of 8,000 cm^3/gmol·s.

Figure 10 shows the solid and gas concentration profiles along the reactor. It is seen that both the solid and gas concentrations drop sharply along the reactor. Figure 11 shows the radial concentration distributions of the solid reactant and the gas reactant as a function of the axial distance. It is seen that, at a given particle radial distance, the radial variation of the solid reactant concentration remains unchanged or increases with the increase of the axial distance. It is seen, however, that at a given particle radial distance, the radial variation of the gas reactant concentration in the solid particle remains unchanged or decreases with the increase of the axial distance, Figure 11.

The effect of negative values of γ on the gas conversion as a function of three values of D_{eA0}, i.e., 0.001, 0.01, and 0.1 cm^2/s, is shown in Figure 12. In contrast to Figure 8 for positive values of γ, at D_{eA0} as small as 0.001 cm^2/s, the gas conversion decreases as $(-\gamma)$ increases. The effect of $(-\gamma)$ on the gas conversion is substantially reduced as D_{eA0} increases to 0.1 cm^2/s.

Experimental Data and Model Verification

Experimental data on the reactant conversion in the vertical pneumatic transport reactor (Battelle's multisolid fluidized bed reactor) obtained in this study are analyzed based on the present model. As indicated previously, the noncatalytic gas-solid reaction under consideration is the limestone reaction with sulfur dioxide generated from coal combustion. This reaction involves the calcination of limestone and the reaction between calcined limestone and sulfur dioxide as:

$$CaCO_3(s) \rightarrow CaO(s) + CO_2(g) \qquad (I)$$

$$CaO(s) + SO_2(g) + \frac{1}{2}O_2(g) \rightarrow CaSO_4(s) \qquad (II)$$

It has been reported that the latter reaction can be considered as

TABLE 3. NUMERICAL VALUES OF THE PARAMETERS EMPLOYED FOR FIG. 13

a	$= 1$	d_p	$= 16\ \mu m$
m	$= 1$	C_{s0}	$= 0.021\ gmol/cm^3$
n	$= 1$	C_0	$= 3.63 \times 10^{-8} - 4.5 \times 10^{-8}\ gmol/cm^3$
ρ_p	$= 2.5\ g/cm^3$		
ρ_g	$= 0.0004\ g/cm^3$	μ_g	$= 4.5 \times 10^{-4}\ g/cm\cdot s$
D	$= 16.2\ cm$	L	$= 610\ cm$
k_v	$= 0.65 \times 10^5\ cm^3/gmol\cdot s$	ϵ_0	$= 0.532$
D_{eA0}	$= 0.095\ cm^2/s$	γ	$= -0.75$
U_{gs}	$= 850$–$1{,}060\ cm/s$		

the rate-determining step in the overall rate of reaction (Fan et al., 1981). The reaction of calcined limestone and SO_2 is characterized by the substantial increase of molar volume of the limestone particle which results in the reduction of porosity during the course of the reaction. Thus, in the present model simulation of the experimental system, a negative value of γ is used.

The value of the parameters used in this simulation are listed in Table 3. Some of the parameters in the table including D, d_p, a, U_{gs}, ρ_g, C_{s0}, C_0, μ_g, and L are operating variables which are known for a given operation. Note that in the table, the sorbent density, ρ_p of 2.5 g/cm^3 is used, which represents the density of uncalcined limestone particles. The density of the particle would reduce to 1.5 g/cm^3 upon complete calcination in the reactor. It would then increase with the sulfation. The analysis conducted in this study indicates that under the dilute flow conditions, the change in the particle density has practically negligible effect on the hydrodynamic properties of the reactor. Furthermore, since W_s in Eqn. (23) is taken as the uncalcined limestone feed rate, the corresponding density of 2.5 g/cm^3 would only yield an appropriate solid particle volumetric flow rate in the reactor.

The order of the reaction, i.e., m and n, is taken as the first order with respect to the solid reactant concentration and the first order with respect to the gas reactant concentration according to Fan et al. (1981).

ρ_p, ϵ_0, D_{eA0}, k_v and γ are the physical or reactivity properties of the solid reactant. Recently, Fee et al. (1980) and Fan et al. (1981) performed extensive experimental analysis to characterize the physical and reactivity properties of over 30 different limestone/dolomite reactants. The type of reactant used in the present experiment is Greer limestone which was identified as Sorbent 8001 by Fee et al. (1980). The values for k_v and γ used in this study are taken directly from Fan et al. (1981). Note that the solid flow rate for the limestone particles in the reactor, W_s, is the sum of the fresh limestone feed rate which is calculated from the given information of calcium-sulfur molar ratio and the recirculation rate of the spent limestone which is obtained experimentally. The concentration of the solid reactant at the reactor inlet is evaluated from a simple material balance by considering the limestone concentration of the fresh sorbent and that of the recirculated sorbent. It is assumed in this study that the concentration of the solid reactant in the particle at the reactor inlet is uniform.

As described previously, the reactor consists of two sections: dilute section and dense section. The dense section is substantially smaller than the dilute section. However, the dense section provides higher residence time for the fine sorbent than does the dilute section. As given in Table 2, the residence time of the fine sorbent in the dense section for the experimental conditions considered in this study is experimentally measured as about 6 s.

The particle linear velocity and the solid hold-up in the dense section are calculated from the residence time of fine particle, volumetric feed rate of fine particles, and volume of the dense section.

Various types of the entrained particles in the dilute section including limestone, coal ash, coal carbon, and inert material (sand) act independently. The hydrodynamic and mass transfer properties of each type of particle can be evaluated by Eqs. 23 through 30. With the solid flow rate for each type of particles known, the solid hold-ups for these particles can be calculated. Thus, the void fraction of the bed in the dilute section can be evaluated.

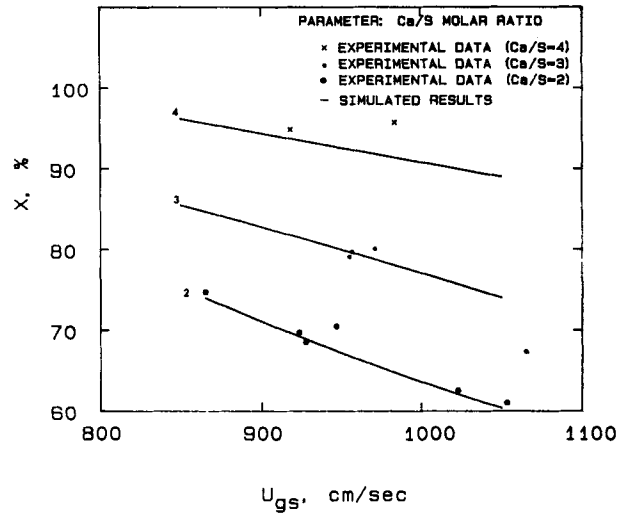

Figure 13. Comparison of the model prediction with experimental data in a plot of X vs. U_{gs}.

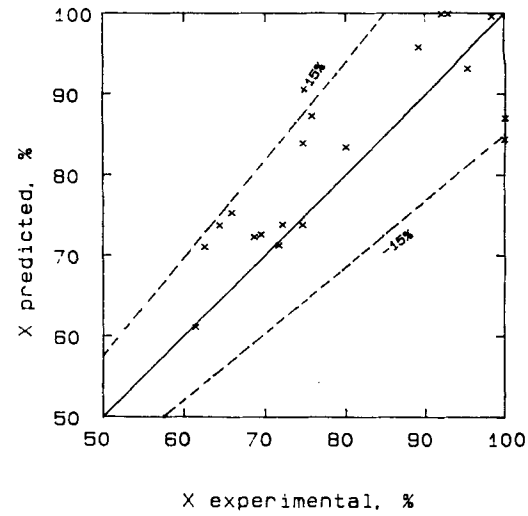

Figure 14. Comparison of the model prediction with additional experimental data in a plot of X, predicted vs. X, experimental.

Equations 1 through 7 are solved separately for dense section and dilute section. The term $(1 - \epsilon_b)$ in Eq. 1 and U_p in Eqs. 3 and 4 are replaced with the solid hold-up and particle linear velocity for each section.

The experimental data and model verifications are presented in Figures 13 and 14. Figure 13 shows the sulfur retention vs. the superficial gas velocity as a function of Ca/S molar ratio for sulfation in the vertical pneumatic transport reactor. Note that variation of Ca/S molar ratio reflects that of Ca circulation rate. It is seen that the comparison between the model prediction and experimental data is satisfactory.

The comparison between the model prediction and additional experimental data is shown in Figure 14. The experimental conditions for Figure 14 are the same as those for Figure 13 except that wider ranges of the gas velocity (385–1,060 cm/s) and the inlet gas reactant concentration (3.3×10^{-8} to 12.8×10^{-8} gmol/cm^3) are considered. It is seen that all the predicted values lie within ±15% of the experimental data.

ACKNOWLEDGMENT

The work performed by L-S Fan and S. Satija was supported by the Battelle Memorial Institute under the University Distribution Program.

NOTATION

A = dimensionless group defined as $\frac{r_0^2 U_p}{L D_{eA0}}$
C_0 = inlet gas reactant concentration (mol/L^3)
C_1 = gas reactant concentration in the gas phase (mol/L^3)
C_2 = gas reactant concentration in the solid phase (mol/L^3)
$\bar{C}_2$ = average gas reactant concentration in the solid phase (mol/L^3)
C_{s0} = initial solid reactant concentration (mol/L^3)
C_s = solid reactant concentration in the solid phase (mol/L^3)
D = inside diameter of the reactor (L)
D_{eA} = effective diffusivity of the gas in the solid particle (L^2/θ)
D_{eA0} = initial effective diffusivity of the gas in the solid particle (L^2/θ)
D_A = D_{eA}/D_{eA0}
D_M = molecular diffusivity in the gas phase (L^2/θ)
d_p = particle diameter (L)
$\mathcal{D}$ = dimensionless group defined as $\frac{3(1-\epsilon_b)LD_{eA}}{U_g \epsilon_b r_0^2}$
E = dimensionless group defined as $\frac{1}{N_{Sha}}$
F = dimensionless group defined as $\frac{3(1-\epsilon_b)k_d L}{U_g \epsilon_b r_0}$
f_1 = C_1/C_0
f_2 = C_2/C_0
f_p = solid friction factor
g_1 = C_s/C_{s0}
G = dimensionless group defined as $\frac{k_v C_0^n L C_{s0}^{m-1}}{U_p}$
g = gravitational acceleration (L/θ^2)
g_c = conversion factor
k_v = volumetric reaction rate constant $L^{3(m+n-1)}/\theta(\text{mol})^{m+n-1}$
k_d = gas film mass transfer coefficient (L/θ)
L = length of the reactor (L)
m = order of reaction with respect to the solid reactant
n = order of reaction with respect to the fluid reactant
N_{Sha} = Sherwood number defined as $\frac{r_0 k_d}{D_{eA0}}$
r = radial position within the solid particle (L)
r_0 = radius of the solid particle (L)
$(Re)_p$ = Reynolds number defined as $d_p(U_g - U_p)\rho_g/\mu$
$(Re)_t$ = Reynolds number defined as $d_p U_t \rho_g/\mu$
Sc = Schmidt number defined as $\mu/\rho_g D_M$
U_g = linear gas velocity (L/θ)
U_{gs} = superficial gas velocity (L/θ)
U_p = linear particle velocity (L/θ)
U_{ps} = superficial particle velocity (L/θ)
V = volume of the solid particle (L^3)
W_s = solid flow rate (M/θ)
X = gas reactant conversion at the reactor outlet
X_s = solid reactant conversion
x = r/r_0
y = z/L
z = axial distance along the reactor (L)

Greek Letters

ϵ_b = void fraction in the reactor
ϵ = void fraction in the solid particle
$\bar{\gamma}_s$ = local solid reaction rate (mol/L^3)
γ = constant defined by Eq. 8
ρ_g = gas density (M/L^3)
ρ_p = particle density (M/L^3)
μ = gas viscosity (M/Lθ)
ϕ_v = $r_0 \sqrt{\frac{a k_v C_{s0}^m C_0^{n-1}}{D_{eA0}}}$

LITERATURE CITED

Bryson, M. C., G. P. Huling, and W. E. Glausser, "Gulf Explores Riser Cracking," *Hydro. Proc.*, **51** (5), 85 (1972).
Currie, T. A., "Gaseous Diffusion in Porous Media. Part 2—Dry Granular Materials," *Brit. J. Appl. Phys.*, **11**, 318 (1960).
Fan, L-S, K. Miyanami, and L. T. Fan, "Transient Analysis in Isothermal Fluid-Solid Reaction Systems—Modeling the Sigmoidial Conversion-Time Behavior of a Gas-Solid Reaction," *Chem. Eng. J.*, **13**, (1), 13 (1977).
Fan, L. T., K. Miyanami, and L-S Fan, "Volume Reaction Model for Fluid-Solid Reactions," *J. Chin. I. Ch. E.*, **12**, 119 (1978).
Fan, L-S, "Modeling of a Vertical Pneumatic Transport Reactor for Catalytic Reactions," 11th Annual Pittsburgh Conf. on Modeling and Simulation, Instrument Society of America, **11**, 1173 (1980).
Fan, L-S, "A Homogeneous Model for Reactant Conversions in a Vertical Pneumatic Transport Reactor for Catalytic Reactions," *Chem. Eng. J.*, **21**, 179 (1981).
Fan, L-S, and S. J. Hwang, "A Heterogeneous Model for Catalytic Reaction in an Isothermal Vertical Pneumatic Transport Reactor," *Chem. Eng. Sci.*, **36** (10), 1736 (1981).
Fan, L-S, S. Satija, I. Wilson, D. Fee, K. M. Myles, and I. Johnson, "Sulfation Kinetics of Calcined Limestones/Dolomites in a Thermogravimetric Analyzer: Experiment, Modeling and Simulation," AIChE 74th Annual Meeting, New Orleans, LA (Nov. 8–12, 1981).
Fee, D. C., W. I. Wilson, J. A. Shearer, J. Lenz, L-S Fan, K. M. Myles and I. Johnson, "Sorbent Utilization Prediction Methodology—Sulfur Control in Fluidized Bed Combustor," ANL/CEN/FE-80-10, Argonne National Laboratory, (Sept., 1980).
Gear, C. W., Numerical Initial Value Problems in Ordinary Differential Equations, Prentice Hall, Englewood, NJ (1971).
Hartman M., and R. W. Coughlin, "Reaction of Sulfur Dioxide with Limestone and the Grain Model," *AIChE J.*, **22**, (3), 490 (1976).
Hartke, W., H. Helmrich, H. Kroger, and K. Schugerl, "Non-Catalytic Decomposition of Sodium Bicarbonate in a Circulating Fluidized Bed Reactor," *Ger. Chem. Eng.*, **4**, 20e (1981).
Nack, H., G. W. Felton, and K. T. Liu, "Battelle's Multisolid Fluidized Bed Combustion Process," 5th Int. Conf. on Fluidized Bed Combustion, Washington, DC, **3**, 223 (Dec., 1977).
Paraskos, J. A., Y. T. Shah, J. D. Mckinney, and N. L. Carr, "A Kinematic Model for Catalytic Cracking in a Transfer Line Reactor," *IEC Proc. Des. Dev.*, **15**, 165 (1976).
Pratt, K. C., "Catalytic Reactions in Transport Reactors," *Chem. Eng. Sci.*, **29**, 747 (1974).
Reh, L., "Calcining Aluminum Trihydrate in a Circulating Fluid Bed, A New Technique," *Proc. Aust. Inst. Min. Met.*, 241 (1972).
Satterfield, C. N., *Mass Transfer in Heterogenous Catalysis*, MIT Press (1969).
Sincovec, R. F., and N. K. Madson, "Software for Nonlinear Partial Differential Equations," *ACM Trans. on Math. Software*, **1** (3), 232 (1975).
Stemerding, S., "Pneumatic Transport of Cracking Catalyst in Vertical Risers," *Chem. Eng. Sci.*, **17**, 599 (1962).
Varghese, P., and A. Verma, "Catalytic Reactions in Transport-Line Reactors," *Chem. Eng. Sci.*, **34**, 337 (1979).
Vichnevetsky, R., "Hybrid Methods for Partial Differential Equations," *Simulation*, 168 (April, 1971).
Wakao, N., and J. M. Smith, "Diffusion in Catalyst Pellets," *Chem. Eng. Sci.*, **17**, 825 (1962).
Weisz, P. B., and A. B. Schwartz, "Diffusivity of Porous-Oxide-Gel-Derived Catalyst Particles," *J. Cat.*, **1**, 399 (1962).
Wen, C. Y., "Non-Catalytic Heterogeneous Solid-Fluid Reaction Models," *I&EC*, **60** (9), 34 (1968).
Yang, W. C., "Estimating the Solid Particle Velocity in Vertical Pneumatic Conveying Lines," *I&EC Fund.*, **12** (3), 349 (1973).
Yang, W. C., "Correlations for Solid Friction Factors in Vertical and Horizontal Pneumatic Conveyings," *AIChE J.*, **20** (3), 605 (1974).
Yang, W. C., "A Unified Theory on Dilute Phase Pneumatic Transport," *J. of Powder & Bulk Solids Tech.*, **1**, 89 (1977).
Yang, W. C., "A Correlation for Solid Friction Factor in Vertical Pneumatic Conveying Lines," *AIChE J.*, **24** (3), 548 (1978).
Yang, W. C., and D. L. Keairns, "Estimating the Acceleration Pressure Drop and the Particle Acceleration Length in Vertical and Horizontal Pneumatic Transport Lines," Pneum. Transport 3, Third Int. Conf. on the Pneumatic Transport of Solids in Pipes, D7-89 (1976).

Manuscript received February 8, 1982; revision received June 24, and accepted January 31, 1983.